A comparative analysis of the TVL1 and the TV-G models

Vincent Duval

A comparative analysis of the TVL1 and the TV-G models

Vincent Duval
CNRS and Université Paris-Dauphine
vincent.duval@ceremade.dauphine.fr

December 14, 2013

Abstract

In this paper, we analyze the fine properties of the minimizers of the TVL1 and the TV-G models used in image processing. We describe the solutions of TVL1 by means of elementary morphological operations, and we exhibit a strong constraint on the structure part and the texture part of the data which is neccessary to obtain exact decompositions using the TV-G model.

For the past two decades, much interest has been given in variational models for image restoration (see [15] and references therein). In the seminal work [64] in image denoising, Rudin, Osher and Fatemi (ROF) proposed to find, given $u \in L^2(\mathbb{R}^2)$, the function u which minimizes the energy

$$\int |Du| + \frac{1}{2\lambda} \int |f-u|^2. \tag{1}$$

Studying the above model in [57], Meyer proposed to replace the L^2 fidelity term with norms which favor oscillations, so as to get a solution u which contains the structure and the geometric features of f, and a residual $f-u$ which contains the oscillating patterns of f, namely the *texture* and possibly some noise.

This new paradigm has lead many researchers to investigate the use of various norms for the fidelity term. To our knowledge, the first attempt to perform numerically such decomposition was made by Vese and Osher in [69] by approximating the G space proposed by Meyer (the divergence of L^∞ vector fields) and the corresponding norm. Another approach to deal with the TV-G model (*i.e.* (1) where the square L^2 norm is replaced with the norm of the G space) is proposed in [18]. Variants of this model using decompositions with three terms (structure, texture and noise) have been investigated in [42, 43]. In [63], another variant of this model is proposed which corresponds to the space $W^{-1,2}$. This approach is generalized in [19, 20], where $TV + \mathcal{H}$ decompositions are considered, with $\mathcal{H}$ a Hilbert space. In this context, negative Sobolev spaces have drawn a lot of attention: see [19, 53, 50]. Two other spaces initially proposed

by Meyer are E (the dual of the Besov space $\dot{B}^1_{1,1}$) investigated in [19, 41], and F (the divergence of vector fields in BMO) studied in [52].

Yet, the search for new fidelity terms did not focus only on oscillating norms, and Chan and Esedoglu considered in [34] the following energy

$$\int |Du| + \lambda \int_{\mathbb{R}^2} |f - u|, \tag{2}$$

importing in image processing a model which had been introduced in signal processing by Alliney [5, 4] and studied by Nikolova [60, 61, 62]. In dimension $N = 1$, an important property of the model, highlighted in [60], is its ability to preserve exactly some signals. In dimension $N \geqslant 2$, this property still holds, but contrary to the dimension $N = 1$, the geometry has a strong influence on the solutions, as studied in [34, 46, 74, 72, 59]. In particular, the link with the flat norm used in geometric measure theory is observed in [59]. Probably, the most remarkable property of this model, observed by Darbon in [36], is its contrast invariance. Namely, if g is an increasing function and u is a solution for data f, $g \circ u$ is a solution associated to $g \circ f$. Such a property is fundamental in image processing, and has been highly considered from the early years of image processing and mathematical morphology (see below) to the axiomatic approach to PDE's in image processing [9, 44] and the tree of shapes studied in [58, 21] (see also [30] and references therein).

Meanwhile, tremendous progress has been made in the understanding of the Rudin-Osher-Fatemi (ROF) model and the total variation flow, thanks to the work of Caselles and his collaborators [13, 12, 14, 22, 23, 8, 28], and to the work of Allard [1, 2, 3]. Giving a rigorous meaning to the total variation flow [13, 12]

$$\frac{\partial u}{\partial t} = \operatorname{div}\left(\frac{Du}{|Du|}\right), \tag{3}$$

Caselles and his coauthors have proved existence and uniqueness of a solution for any initial data $u_0 \in L^2(\mathbb{R}^2)$. The solution vanishes in finite time and, up to a renormalization, it converges to a solution of the eigenvalue problem:

$$u = -\operatorname{div}\left(\frac{Du}{|Du|}\right). \tag{4}$$

The solutions of (4) are the functions which evolve at constant speed in (3) and the functions that evolve in (1) by the multiplication of a constant. Focussing on characteristic functions of sets which satisfy (4), the authors of [22, 23] were lead to study the class of calibrable sets. It turns out that these sets are intimately linked with the so-called *Cheeger sets*. Given a domain Ω, a Cheeger set of Ω is a solution to the problem

$$\inf_{E \subseteq \Omega} \frac{\operatorname{Per} E}{|E|}, \tag{5}$$

where $|E|$ is the N-dimensional Lebesgue measure of E and $\operatorname{Per} E$ its perimeter (see below). If the domain Ω is convex, Ω is itself a solution to (5) if and only

if it is calibrable (see [15]). The deep results in [8, 7] and later in [29, 6] yield a characterization of Cheeger sets in convex domains by their mean curvature, as well as a uniqueness result for non trivial convex bodies (*i.e.* convex compact sets with nonempty interior). They also describe precisely the evolution of convex sets by the total variation flow (eq. (3)) and the Rudin-Osher-Fatemi problem (eq. (1)). Independently, Allard has also proposed a thorough study of the models TV+L^p ($p \geqslant 1$) in [1, 2, 3], obtaining similar results, notably in the case of convex sets.

The present paper summarizes several results developed in the PhD thesis [38]. Our purpose is to describe as precisely as possible the solutions of the TVL1 (eq. (2)) and the TV-G models. In particular, we relate the TVL1 model with morphological openings, and we give examples of structure-texture decomposition using the TV-G model. Incidentally, the proposed results provide an extension of the comparison initiated by Haddad in [46] and Yin *et al.* in [73] between both models. Whereas [46] emphasizes the similitudes between the two models, we highlight fine properties of the minimizers which make the models eventually different. An illustration is given in Figure 1. Both models are able to separate the stripes from the clothes, but the solution provided by the TV-G model looks more *inflated* than the one of the TVL1 model (which looks *flat*). Our analysis gives some insight on the qualitative difference between both results.

The first section deals with preliminaries and notations. The second one is devoted to the TVL1 model, and it covers material published in [39]. Relying on the deep results mentioned above (in particular [23, 8, 7]) we show the link between TVL1 and the Cheeger problem, and we obtain a characterization of the solutions in terms of morphological openings. This provides some insight on the behavior of the solutions as well as a way to compute approximations of solutions by means of classical morphological operators. Moreover it explains the good behavior of the model for structure-texture decomposition. In the third section, we analyze the TV-G model. After recalling the characterization of solutions, we exhibit toy examples which predict a perfect decomposition between structure and texture. Then we point out a limitation of the model which prevents perfect decompositions to happen in the general case: oscillations must appear in the texture part around the edges of the image. This phenomenon, which explains the *inflated* look of the decompositions, does not affect the TVL1 model.

1 Preliminaries

1.1 Functions of bounded variations

We briefly recall some properties of functions of bounded variations and sets of finite perimeter. We refer the reader to [11] for a comprehensive treatment of the subject.

Definition 1. *A function $u \in L^1(\mathbb{R}^2)$ is said to be of bounded variation if its distributional gradient is a vector valued Radon measure with finite total*

Figure 1: Decomposition of the famous "Barbara" image using the algorithm in [18] (top) and TVL1 (bottom).

variation. The total variation of Du on an open set $\Omega \subset \mathbb{R}^2$ is equal to:

$$|Du|(\Omega) = \sup\left\{ \int_{\mathbb{R}^2} u \operatorname{div} \varphi / \ \varphi \in C_c^1(\Omega, \mathbb{R}^2), \forall x \in \Omega, \ |\varphi(x)| \leqslant 1 \right\} \tag{6}$$

(where for $v = (v_1, v_2) \in \mathbb{R}^2$, $|v|^2 = v_1^2 + v_2^2$). When $\Omega = \mathbb{R}^2$, this quantity is called the total variation of u, and will be denoted by $\int |Du|$ or $|u|_{TV}$.

The mapping $u \mapsto |Du|(\Omega)$ is $L^1_{loc}(\mathbb{R}^2)$ lower semi-continuous.

If E is a measurable set, we denote by $|E|$ the 2-dimensional Lebesgue measure of a set $E \subseteq \mathbb{R}^2$, and by $\mathcal{H}^1(E)$ its 1-dimensional Hausdorff measure in $\mathbb{R}^2$. The set E is said to be of finite perimeter if (6) is finite (with $\Omega = \mathbb{R}^2$) when u is replaced with the characteristic function $\mathbf{1}_E$ of E. Its perimeter is defined as $\operatorname{Per} E = \int |D\mathbf{1}_E|$.

If $E \subseteq \mathbb{R}^2$ is a Lebesgue measurable set, and $x \in \mathbb{R}^2$, the upper and lower densities of E at x are respectively defined by:

$$\overline{D}(x, E) := \limsup_{r \to 0} \frac{|B(x,r) \cap E|}{|B(x,r)|}, \quad \underline{D}(x, E) := \liminf_{r \to 0} \frac{|B(x,r) \cap E|}{|B(x,r)|},$$

where $B(x,r)$ is the Euclidean closed ball with radius $r > 0$ and center x. Lebesgue's density theorem states that for any measurable set E both quantities are equal to 1 at almost every point of of E. Hence, the set $\{x \in \mathbb{R}^2, \ \overline{D}(x, E) = \underline{D}(x, E) = 1\}$ is a Lebesgue representative of E, independent of the choice of representative for E. We shall choose this precise representative, and ∂E, $\mathring{E}$ shall refer respectively to the topological boundary and interior of this representative.

Following the framework of [15], we rely on the results of [16] for a generalization of the Gauss-Green theorem. Let $\Omega \subseteq \mathbb{R}^2$ be an open subset, and for $p \in [1, +\infty]$,

$$X_p(\Omega) := \{ z \in L^\infty(\Omega, \mathbb{R}^2), \ \operatorname{div} z \in L^p(\Omega) \}. \tag{7}$$

If $z \in X_p(\Omega)$ and $w \in L^q(\Omega) \cap \mathrm{BV}(\Omega)$ with $p^{-1} + q^{-1} = 1$, we define the functional $(z, Dw) : C_c^\infty(\Omega) \to \mathbb{R}$ by the formula:

$$\langle (z, Dw), \varphi \rangle := -\int_\Omega w\varphi \operatorname{div} z dx - \int_\Omega wz \cdot \nabla\varphi dx. \tag{8}$$

In fact, (z, Dw) is a Radon measure in Ω, and for all Borel set $B \subset \Omega$:

$$\left| \int_B (z, Dw) \right| \leqslant \int_B |(z, Dw)| \leqslant \|z\|_\infty \int_B |Dw|. \tag{9}$$

Moreover, if $w \in L^q(\Omega) \cap W^{1,1}$, $\int_\Omega (z, Dw) = \int_\Omega z \cdot \nabla w dx$.

The following theorem is proved in [16]:

Theorem 1. *Let $\Omega \subset \mathbb{R}^2$ be a bounded open set with Lipschitz boundary. Let $u \in BV(\Omega) \cap L^q(\Omega)$ and $z \in X_p(\Omega)$. Then there exists a function $[z \cdot \nu^\Omega] \in L^\infty(\partial\Omega)$ such that $\|[z \cdot \nu^\Omega]\|_{L^\infty(\partial\Omega)} \leqslant \|z\|_{L^\infty(\Omega, \mathbb{R}^2)}$, and*

$$\int_\Omega u \operatorname{div} z dx + \int_\Omega (z, Du) = \int_{\partial\Omega} [z \cdot \nu^\Omega] u d\mathcal{H}^1.$$

When $\Omega = \mathbb{R}^2$, we have the following formula [16], for $z \in X_p(\mathbb{R}^2)$ and $w \in L^q(\mathbb{R}^2) \cap \mathrm{BV}(\mathbb{R}^2)$:

$$\int_{\mathbb{R}^2} w \operatorname{div} z dx + \int_{\mathbb{R}^2} (z, Dw) = 0. \tag{10}$$

Using the above integration by parts, it is possible to describe the subdifferential $\partial|\cdot|_{TV}$ of the total variation. This is done in particular in [13, 15] in order to define the meaning of the total variation flow. Let $p \in L^\infty(\mathbb{R}^2)$, then $p \in \partial|\cdot|_{TV}(u)$ if and only if there exists $z \in L^\infty(\mathbb{R}^2, \mathbb{R}^2)$ such that

$$\|z\|_\infty \leqslant 1,\ p = -\operatorname{div} z \text{ and } \int_{\mathbb{R}^2} -\operatorname{div} z(x)u(x)dx = \int |Du|. \tag{11}$$

In view of (10), the last equality may be rewritten $\int_{\mathbb{R}^2}(z, Du) = \int |Du|$.

1.2 The G-space

Yves Meyer introduced the G-space in [57] while studying the ROF problem, so as to model oscillating patterns like textures. Several variants of the definition have been used in the literature (see [17] for a definition on a bounded domain), we adopt the one in [51].

Definition 2. *A function $f \in L^2(\mathbb{R}^2)$ belongs to G if and only if there exists a vector field $g \in L^\infty(\mathbb{R}^2, \mathbb{R}^2)$ such that* $\operatorname{div} g = f$. *The G-norm is defined as:*

$$\|f\|_G := \inf\left\{\|g\|_\infty,\ f = \operatorname{div} g, g \in L^\infty(\mathbb{R}^2, \mathbb{R}^2)\right\}. \tag{12}$$

In fact, this infimum is a minimum, i.e. there exists $g \in L^\infty(\mathbb{R}^2, \mathbb{R}^2)$ such that $\operatorname{div} g = f$ *and $\|g\|_\infty = \|f\|_G$. In that case we say that g is adapted to v.*

The G-norm can alternatively be written in a "dual" form (see [47, 51]),

$$\|f\|_G = \sup_{u \in \mathrm{BV}(\mathbb{R}^2)\setminus\{0\}} \frac{\int_{\mathbb{R}^2} fu}{\int |Du|}. \tag{13}$$

The G-norm defines a coarser topology than the L^2 norm. More precisely, it is proved in [47, 51] that $\|f\|_G \leqslant \frac{1}{2\sqrt{\pi}}\|f\|_2$ for all $f \in L^2(\mathbb{R}^2)$. The main motivation for introducing the G-norm is indeed that it does not penalize oscillating patterns. For instance, as explained in [57], if $f(x_1, x_2) = \mathbf{1}_{[0,1]^2}(x_1, x_2)\cos(N\pi x_1)$, then $\|f\|_G = \frac{1}{N}$. More generally,

Proposition 1 ([47], Corollary 3.4)**.** *Let $Q = [0,1]^2$, $f \in L^2(\mathbb{R}^2)$ and $\mu \in L^\infty(\mathbb{R}^2)$ such that $\int_{Q+k} \mu(x)dx = 0$, for all $k \in \mathbb{Z}^2$. Then, $\|f(\cdot)\mu(N\cdot)\|_G \to 0$ when $N \to +\infty$.*

Following the method used in [15] to characterize the subdifferential of the total variation, we may compute the subdifferential of the G-norm by observing that it is the support function of the closed convex set $A = \{u \in L^2(\mathbb{R}^2), \int |Dv| \leqslant 1\}$. Thus, given $p \in L^2(\mathbb{R}^2)$, $u \in G$,

$$p \in \partial\|\cdot\|_G(u) \text{ if and only if } \int |Dp| \leqslant 1 \text{ and } \int_{\mathbb{R}^2} p(x)u(x)dx = \|u\|_G. \tag{14}$$

1.3 Mathematical morphology

Mathematical morphology is a theory of image analysis initiated by Matheron and Serra in the 1960's. Its main focus is the contrast-invariance in image processing, and the consequence is that morphological operators can be equivalently seen as operators on functions (images) or on sets (their level-sets). For instance, some of the most famous morphological operators are respectively the erosion and dilation: for $X \subseteq \mathbb{R}^2$,

$$\mathcal{E}_r X = \left\{x \in \mathbb{R}^2, B(x,r) \subset X\right\}, \quad \mathcal{D}_r X = \left\{y \in \mathbb{R}^2, \exists x \in E,\ y \in B(x,r)\right\}, \tag{15}$$

where $r > 0$ and $B(x,r)$ is the Euclidean closed ball with radius r. These operators on sets are associated with functional operators:

$$\forall u \in \mathbb{R}^{\mathbb{R}^2},\ \forall x \in \mathbb{R}^2, \quad E_r u(x) = \inf_{y \in B(0,r)} u(x+r), \quad D_r u(x) = \sup_{y \in B(0,r)} u(x+r). \tag{16}$$

As a matter of fact, it is equivalent to apply each functional operator to a function f or to apply the corresponding set operator on the upper level-sets of f, $F_t = \{x \in \mathbb{R}^2, f(x) \geqslant t\}$, to obtain sets U_t for $t \in \mathbb{R}$ and then reconstruct u by the formula:

$$\forall x \in \mathbb{R}^2, \quad u(x) = \sup\{t \in \mathbb{R},\ x \in U_t\}. \tag{17}$$

From dilations and erosions, two other basic operators are constructed: openings (defined as $D_r \circ E_r$) and closings (defined as $E_r \circ D_r$). The corresponding set operators may be written as: for $X \subseteq \mathbb{R}^2$,

$$\mathcal{O}_r X = \bigcup\{B(x,r),\ B(x,r) \subset X\}, \quad \mathcal{C}_r X = \Big(\bigcup\{B(x,r),\ B(x,r) \subset X^C\}\Big)^C, \tag{18}$$

where $X^C = \mathbb{R}^2 \setminus X$.

Standard references about mathematical morphology are the book by Matheron [55] and those by Serra [65, 66]. From the fundamental axioms established by Matheron and Serra, and the basic operations such as erosions, dilations, openings and closings, mathematical morphology has grown into a well-established theory from which derive algorithms for image denoising [35, 70], segmentation [25, 26], texture analysis [68, 48], etc.

2 A geometric characterization of solutions for TVL1 model

2.1 A geometric equivalence property

Given $f \in L^1(\mathbb{R}^2)$, the TVL1 model consists in solving the variational problem

$$\inf_{u \in \mathrm{BV}(\mathbb{R}^2)} \left\{ \int_{\mathbb{R}^2} |Du| + \lambda \int_{\mathbb{R}^2} |f-u| \right\}. \tag{$\mathcal{P}_\lambda(f)$}$$

Existence of a solution follows from the direct method of the calculus of variations. Since the problem is not strictly convex, Problem $(\mathcal{P}_\lambda(f))$ may have more than one solution.

Following the fruitful approach of [32, 7] for the study of the Rudin-Osher-Fatemi problem, Chan and Esedoglu have observed in [34] (see also [37]) that the energy in $(\mathcal{P}_\lambda(f))$ may be written as a sum of energies for the level sets of u,

$$\int |Du| + \lambda \int |f-u| = \int_{-\infty}^{+\infty} \operatorname{Per} U_t + \lambda |U_t \Delta F_t| dt, \tag{19}$$

where $U_t = \{x \in \mathbb{R}^2, u(x) \geqslant t\}$ denotes the t-upper level set of u and $F_t = \{x \in \mathbb{R}^2, u(x) \geqslant t\}$ is the t-upper level set of F.

This consequence of the coarea formula has lead several authors (see [34, 37, 74, 1, 39]) to study the connection between $(\mathcal{P}_\lambda(f))$ and the geometric problem

$$\inf_{U \subseteq \mathbb{R}^2} \operatorname{Per} U + \lambda |U \Delta F| \tag{$\mathcal{G}_\lambda(F)$}$$

where $F \subseteq \mathbb{R}^2$ is a measurable set such that $\mathcal{L}^2(F) < +\infty$ or $\mathcal{L}^2(\mathbb{R}^2 \setminus F) < +\infty$.

In fact, applying the general method detailed in [33], one may show that *$u \in L^1(\mathbb{R}^2)$ is a solution to $(\mathcal{P}_\lambda(f))$ if and only if for all $t \in \mathbb{R}$, its level set U_t is a solution to $\mathcal{G}_\lambda(F_t)$, where $F_t = \{x \in \mathbb{R}^2, u(x) \geqslant t\}$.*

Instead of solving $(\mathcal{P}_\lambda(f))$, one may study the solutions of $\mathcal{G}_\lambda(F_t)$ for all $t \in \mathbb{R}$, and then reconstruct u by the formula:

$$u(x) = \sup \{t \in \mathbb{R},\ x \in U_t\}, \tag{20}$$

as done in [74, 1, 59, 39].

2.2 TVL1 Geometric Measure Theory

A remarkable property of Problem $(\mathcal{G}_\lambda(F))$ is the fact that its solutions have smooth boundary. This was derived by Allard in [1], and independently in [39, 38] by the present author with coauthors by applying results from [10].

Proposition 2. *Let $F \subseteq \mathbb{R}^2$, and let $U \in \mathbb{R}^2$ be a solution of $\mathcal{G}_\lambda(F)$. Then ∂U is a $C^{1,1}$ hypersurface. Its curvature κ is defined $\mathcal{H}^1$-almost everywhere and for $\mathcal{H}^1$-almost every $x \in \mathring{F}$ (resp. $x \in \overbrace{(\mathbb{R}^2 \setminus F)}^{\circ}$), $\kappa(x) = -\lambda$ (resp. $+\lambda$). Moreover for $\mathcal{H}^1$-a.e. $x \in \partial U$, $|\kappa(x)| \leqslant \lambda$.*

An interpretation of Proposition 2 is that as soon as ∂U drifts away from ∂F, it is made of arcs of circles with radius $\frac{1}{\lambda}$.

The enlightening example of the union of two discs is studied in [3, 31] (see Figure 2). It is shown that for two discs that are sufficiently close to each other, the solution is either the two disc, the empty set or the figure obtained by joining the discs with arcs of radius $\frac{1}{\lambda}$, depending on the value of λ.

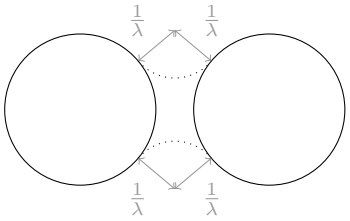

Figure 2: Two discs interact with arcs of circles of radius $\frac{1}{\lambda}$

In contrast with the above example, some sets F do not evolve when solving $\mathcal{G}_\lambda(F)$ for large values of λ, and then suddenly vanish when λ is below a certain threshold λ_F. This is for instance the case of a single disc, as studied in [34]. As we observed in [39], such sets are necessarily *Cheeger in themselves*.

Proposition 3. *Let $F \subseteq \mathbb{R}^2$ be a nonempty set such that there exists $\lambda_F > 0$ such that*

- *F is a solution of $\mathcal{G}_\lambda(F)$ for $\lambda > \lambda_F$,*
- *$\emptyset$ is a solution of $\mathcal{G}_\lambda(F)$ for $\lambda < \lambda_F$.*

Then, $\lambda_F = \frac{\operatorname{Per} F}{|F|}$, and F is Cheeger in itself, i.e. it is a solution of the problem

$$\inf_{U \subseteq F} \frac{\operatorname{Per} U}{|U|}. \tag{$\mathcal{C}(F)$}$$

Moreover, the solution to $\mathcal{G}_\lambda(F)$ for $\lambda \neq \lambda_F$ is unique, and both $\emptyset$ and F are solutions to $\mathcal{G}_{\lambda_F}(F)$.

As we shall see below, the connection between the TVL1 problem and the Cheeger problem is in fact very deep, just as it is for the ROF problem (see for instance [23, 7, 27]).

In the particular case where F is convex, $\operatorname{Per}(U \cap F) \leqslant \operatorname{Per} U$ for all $U \subset \mathbb{R}^2$ with finite perimeter. Hence we may assume that the solution $U \subseteq F$, and Problem ($\mathcal{G}_\lambda(F)$) is then equivalent to

$$\inf_{U \subseteq F} \operatorname{Per} U - \lambda |F|. \tag{$\mathcal{G}'_\lambda(F)$}$$

This family of problems is precisely the one that appears naturally in the study of both the Cheeger problem and the ROF problem when the input is $f = \mathbf{1}_F$ with F convex. The characterization of the solutions to these problems by their curvature and ratio perimeter/area is given in [7], and the link between the curvature of a convex set and its invariance by openings in [13]. It is used in [8] (and independently in [49]) to characterize the solutions of the Cheeger problem: if F is a convex set, the solution to Problem ($\mathcal{C}(F)$) is given by the morphological opening $\mathcal{O}_{1/\lambda^*}F = \bigcup\{B(x, \frac{1}{\lambda^*}), x \in F \text{ and } B(x, \frac{1}{\lambda^*}) \subseteq F\}$ for some value λ^* characterized by $\frac{\operatorname{Per} \mathcal{O}_{1\lambda^* F}}{|\mathcal{O}_{1/\lambda^* F}|} = \frac{1}{\lambda^*}$.

Concatenating these results, we observed in [39]:

Theorem 2 (Solution for convex data)**.** *Let $F \subseteq \mathbb{R}^2$ be a nonempty bounded convex set, and let $\lambda^* > 0$ defined above. The set of solutions to $\mathcal{G}_\lambda(F)$ is*

- $\{\mathcal{O}_{1/\lambda}F\}$ *for* $\lambda > \lambda^*$,
- $\{\emptyset, \mathcal{O}_{1/\lambda^*}F\}$ *for* $\lambda = \lambda^*$ *(where* $\mathcal{O}_{1/\lambda^*}F$ *is the Cheeger set of* F*),*
- $\{\emptyset\}$ *for* $\lambda < \lambda^*$.

2.3 Link with Mathematical Morphology

The fact that TVL1 is a morphological filter (*i.e.* contrast invariant and idempotent) is a consequence of the geometric equivalence property. It was first noticed in [36], and several related properties were independently observed in [74].

Proposition 4 ([36, 74])**.** *Let* $f \in L^1(\mathbb{R}^2)$, $u \in \mathrm{BV}(\mathbb{R}^2)$.

- *For all* $\tau \in \mathbb{R}^2$, $u(\cdot - \tau)$ *is a solution to* $\mathcal{P}_\lambda(f(\cdot - \tau))$ *if and only if* u *is a solution to* $\mathcal{P}_\lambda(f)$
- *For all Lipschitz homomorphism* $g : \mathbb{R} \to \mathbb{R}$, $g \circ u$ *is a solution to* $\mathcal{P}_\lambda(g \circ f)$ *if and only if* u *is a solution to* $\mathcal{P}_\lambda(f)$.

The second point of Proposition 4 not only means that the filter is invariant by contrast change, but also that it is self-dual (choosing $g = -\mathrm{Id}$). All these axioms of mathematical morphology (see [65, 44]) satisfied by the model strongly advocate for its use in image processing.

The main interest of Theorem 2 is that it gives the explicit form of the morphological operator involved (at least when the level sets of f are convex). Since $\lambda > \lambda^*$ is equivalent to $\frac{\mathrm{Per}\,\mathcal{O}_\lambda F}{|\mathcal{O}_\lambda F|} < \lambda$, the solution to TVL1 amounts in this case to a morphological opening, and a "thresholding" on the ratio perimeter/area of the result: if it is greater than λ, the level set should be replaced with $\emptyset$ (see Section 2.4). The theorem also highlights the importance of the scale of objects in the behavior the model.

The notion of scale is intrinsically linked with the development of mathematical morphology. In order to measure the petrographic distribution of oolites and chlorite cement in Lorraine iron ores (see [56]) Matheron and Serra have introduced operations like erosions, dilations and openings and defined the concept of granulometry that allows to discriminate objects by their size (see [54, 45]). Since then, the use of mathematical morphology and granulometries has spread to various areas of image processing especially in the study of textures in general [67] (an example is shown in Figure 3).

Definition 3. *A granulometry is a family of openings* $\{\gamma_\mu\}$ *depending on a positive parameter* μ*, that are decreasing functions with respect to* μ*:* $\mu_2 \geqslant \mu_1 > 0 \Rightarrow \gamma_{\mu_2} \leqslant \gamma_{\mu_1}$. *The cumulative size distribution of a set* F *is* $\mu \mapsto 1 - \frac{|\gamma_\mu F|}{|F|}$. *Its derivative is called the granulometric spectrum of* F*:* $-\frac{1}{|F|}\frac{d}{d\mu}|\gamma_\mu F|$.

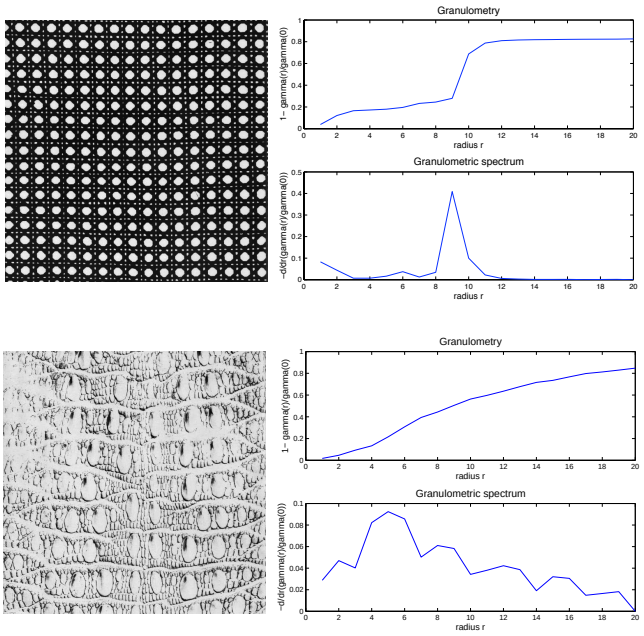

Figure 3: Examples of granulometries. The granulometric spectrum indicates the characteristic scales of the image.

Recently, a similar approach was introduced by Vixie *et al.* (see [71]) in order to classify shapes using TVL1. Introducing (among other signatures) the *shape signature* $s_F : \lambda \mapsto \frac{|U_\lambda \Delta F|}{|F|}$ where U_λ is a solution to $\mathcal{G}_\lambda(F)$, they plot $\lambda \mapsto s_F(\frac{1}{\lambda})$, and they show that this curve gives information about the scales of the object F. In particular, they notice the importance of the jumps of s_F and they propose to examine the derivative $\lambda \mapsto \frac{d}{d\lambda} s_F(\frac{1}{\lambda})$.

This is precisely the philosophy of granulometries and granulometric spectra, and Theorem 2 shows that the examined quantities are in fact almost the same.

2.4 An Algorithm using the Fast Level Set Transform

In order to numerically compare the solutions of TVL1 with the result of openings, we have built an algorithm which is based on the Fast Level Set Transform (FLST) introduced in [58]. A shape is defined as the union of a connected component of an upper or lower set together with its holes. Monasse and Guichard have proved in [58] that, in the discrete framework, shapes have a tree structure for the inclusion relation (which was extended in [21] by Ballester *et al.* to the continuous case), and they have proposed a fast algorithm to compute it. More detail about the tree of shapes can be found in the book by Caselles an Monasse [30].

We only sketch the principle of our algorithm, and we refer the reader to [39] for more detail.

From Theorem 2 (which only deals with convex sets) and the self-duality of the model, we infer that the result of TVL1 is similar to a closing in locally concave parts. The example of the two discs (see Figure 2) is also in favor of such a behavior. A good compromise between openings with radius $1/\lambda$ in convex regions and closings in concave parts is given by the alternate sequential filter (ASF). This filter consists, given a small value r_0, in performing alternatively an opening and a closing of radius nr_0 until $nr_0 \geqslant 1/\lambda$. When r_0 is small enough, the operator is much more symmetric than a single opening-closing step, and starting with either an opening or a closing makes little difference.

The openings and closings are computed for all level sets simultaneously by using their formulation for functions. Then, the "thresholding" on the ratio perimeter/area is adapted by testing whether the energy of the connected component is less than the energy of the empty set (this variation of energy is denoted by $\Delta\mathbb{E}$). The advantage of using the fast level set transform is that the procedure is automatically self-dual and that it allows to deal with all similar level sets at a time. The algorithm is summarized in Figure 4.

A visual comparison with a gradient descent is given in Figure 5. The result are quite similar but since the coarea formula does not hold for the discretized isotropic total variation, the latter yields a blurry image. We have also compared our procedure with the graph-cut algorithm by Darbon and Sigelle [37]. The total variation is then an anisotropic total variation. It is proved in [38] by relying on results from [24], that Theorem 2 holds for crystalline anisotropic total variations when replacing balls with the Wulff shape (see [38] for more details). Here, the openings with balls are replaced with openings with squares of side $2/\lambda$. The similarity between the exact result [37] and the result of the FLST-based algorithm is striking.

3 The TVG model

Observing the behavior of the G-norm for oscillating functions, Y. Meyer proposed to use the G space to model textures, decomposing an image $f \in L^2(\mathbb{R}^2)$ into a structure (or *cartoon*) part u and a texture part $v = f - u$ using the following variational problem:

$$\inf_{u \in \mathrm{BV}(\mathbb{R}^2)} \int |Du| + \lambda \|f - u\|_G. \qquad (\mathcal{Q}_\lambda(f))$$

The existence of a solution follows from the direct method of the calculus of variations. The solution to $\mathcal{Q}_\lambda(f)$ is not necessarily unique (see [47]). Kindermann, Osher and Xu have characterized the optimality of solutions for $\mathcal{Q}_\lambda(f)$ in [51]. Using the subdifferential of the G-norm derived in (14), we may obtain the same result straightforwardly, writing $0 \in \partial|\cdot|_{TV}(u) + \lambda\partial\|\cdot\|_G(f-u)$.

Algorithm FLST-based TVL1

Inputs: Image f
Parameters: Fidelity parameter λ
Output: Approximate solution u

Perform Alternate Sequential Filter: $a := ASF(f)$
Compute the Level Set Transform: $T := FLST(a)$
for all shape s of the tree T **do**
  Remove the children t of s such that $V_t = V_s$.
  if $(\Delta\mathbb{E} < 0)$ **then**
    Remove s.
  end if
end for
Reconstruct $u := FLST^{-1}(T)$.

Figure 4: An algorithm to compute an approximate solution of TVL1 using openings and the Fast Level Set Transform. The tree is visited from the leaves to the root.

Proposition 5 ([51])**.** *The decomposition (u, v) is optimal if and only if:*

$$\exists z \in X_\infty, \quad |z| \leqslant 1 \text{ and } -\int u \operatorname{div} z = \int |Du|, \tag{21}$$

$$\exists p \in \mathrm{BV}(\mathbb{R}^2), \quad \int |Dp| \leqslant 1 \text{ and } \int pv = \|v\|_G, \tag{22}$$

$$\text{such that} \quad -\operatorname{div} z + \lambda p = 0. \tag{23}$$

Haddad and Meyer have studied the case where the whole signal is in the texture part ($u = 0$, $v = f$). Conversely they have also proved that if $\int |Dp| < 1$ in (22), the solution must be $(u, v) = (f, 0)$. Let us also mention that they have deeply investigated the radial case using Proposition 5, expliciting in particular the decomposition of the radial function $f(r) = e^{-r}$.

The *rationale* behind Problem $(\mathcal{Q}_\lambda(f))$ is of course that if an image f is the sum of a structure part and a texture part, one expects to get the former in the solution u of $Q_\lambda(f)$ part and the latter in $v = f - u$. Indeed, the total variation is low for *cartoon*-like images and high for oscillating images, and conversely for the G-norm. This approach has had a certain success in practical applications (see [18, 73, 42]).

The aim of this section is to discuss the limitations of the above paradigm. *Can this model actually separate texture from structure? Is there any constraint on the texture and structure part?*

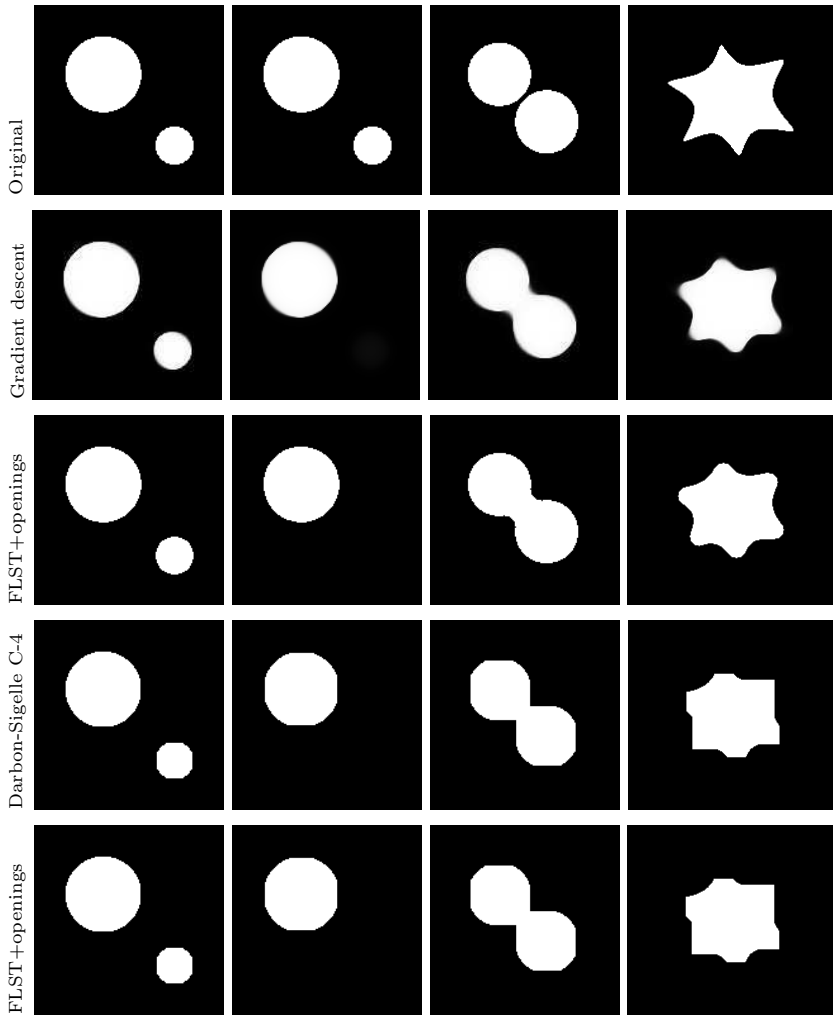

Figure 5: **First row:** original image. **Second row:** result of a gradient descent scheme. **Third row:** result of the FLST-based algorithm with euclidean balls as structuring elements. **Fourth row:** result obtained with Darbon-Sigelle's algorithm (connectivity 4). **Five row:** result of the FLST based algorithm, using a square as structuring element. All pictures were computed with $\lambda = 1/9$, except the first column ($\lambda = 1/6$, the small component is kept, contrary to the second column).

3.1 When it works...

Let (u, v) be a decomposition of f using $(\mathcal{Q}_\lambda(f))$. If $v \neq 0$, then $\int |Dp| = 1$ in (22) according to [47]. Now, let $g \in L^\infty(\mathbb{R}^2, \mathbb{R}^2)$ be a vector field adapted to v, *i.e.* $\operatorname{div} g = v$ and $\|g\|_\infty = \|v\|_G$. By integration by parts, (22) is equivalent to

$$-\int (g, Dp) = \|g\|_\infty \int |Dp|, \quad \text{i.e.} \quad 0 = \int \left((g, \frac{Dp}{|Dp|}) + \|g\|_\infty \right) d|Dp|. \quad (24)$$

This means that $|Dp|$-almost everywhere, $|g|$ must reach its maximum, and g must be pointing in the opposite direction from Dp. To build examples of exact decompositions, it is therefore sufficient to define vector fields z and g which satisfy (24) with $p = -\frac{1}{\lambda} \operatorname{div} z$.

In the radial case, we have proved in [38] the following result which guarantees a successful decomposition. Let us write $z(x) = \tilde{z}(r)e_r$, $g(x) = \tilde{g}(r)e_r$, $u(x) = \tilde{u}(r)$, *etc.*

Proposition 6. *Let $\tilde{g} \in W^{1,\infty}(\mathbb{R}_+, \mathbb{R})$ with $\tilde{g}(0) = 0$. Assume that there are values $0 < r_{j^*} < \ldots < r_0 < \ldots < r_{k^*}$ with $r_0 = 1$ such that $\tilde{g}(r_k) = (-1)^{k+1}\|\tilde{g}\|_\infty$ for $k \in \{j^*, \ldots 0, \ldots k^*\}$ and $r_{k+1} - r_k \leqslant r_k$ for $j^* \leqslant k \leqslant k^* - 1$. Then, for*

$$4\pi \leqslant \lambda \leqslant 4\pi \left(1 + \sum_{k=j^*}^{k^*-1} \frac{r_{k+1} + r_k}{r_{k+1} - r_k} \right), \quad (25)$$

the radial function f defined by $\tilde{f}(r) = \mathbf{1}_{[0,1]}(r) + \beta \frac{1}{r} \frac{\partial r\tilde{g}(r)}{\partial r}$ has a perfect decomposition (u, v) given by:

$$\begin{cases} \tilde{u}(r) &= \mathbf{1}_{[0,1]}(r) \\ \tilde{v}(r) &= \beta \frac{1}{r} \frac{\partial r\tilde{g}(r)}{\partial r} \end{cases}.$$

Here is a typical example of the result. Let $N \in \mathbb{N}^*$ be an odd number, and consider the function f defined by

$$\tilde{f}(r) = \mathbf{1}_{[0,1]}(r) - \beta \left(\sin(N\pi r) - \frac{1}{\pi N r} \cos(N\pi r) \right) \mathbf{1}_{[1/2,3/2]}(r),$$

so that we may choose $r_k = 1 + \frac{k}{N}$ and $k^* = -j^* = \frac{N-1}{2}$.

For $4\pi \leqslant \lambda \leqslant 4\pi \left(2N^2 - 2N + 1\right)$, f has an optimal decomposition given by:

$$\tilde{u}(r) = \mathbf{1}_{[0,1]}(r),$$
$$\tilde{v}(r) = -\beta \left(\sin(N\pi r) - \frac{1}{\pi N r} \cos(N\pi r) \right) \mathbf{1}_{[1/2,3/2]}(r).$$

This decomposition is illustrated in Figure 6 and the constructed z and p are shown in Figure 7. Incidentally, let us observe the effect of the frequency (N or $\frac{1}{r_{k+1} - r_k}$ above) on the decomposition: the faster the oscillation, the larger the interval of λ for which the decomposition is perfect.

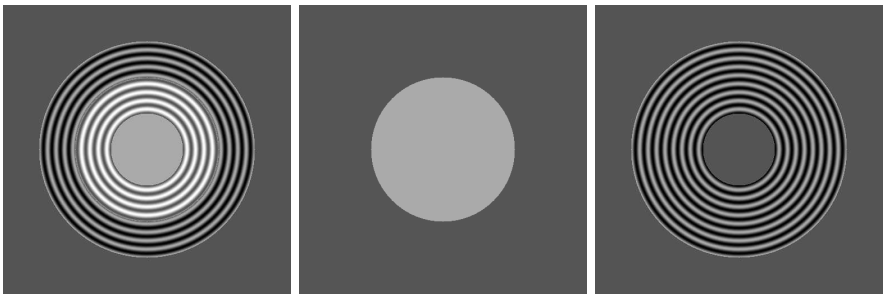

Figure 6: TV-G decomposition predicted by Proposition 6: original image f (left), cartoon part $u = \mathbf{1}_{B(0,1)}$ (middle), texture part $v(x) = \left(-\sin(N\pi|x|) + \frac{1}{\pi N}\cos(N\pi|x|)\right)\mathbf{1}_{[1/2,3/2]}(|x|)$ (right).

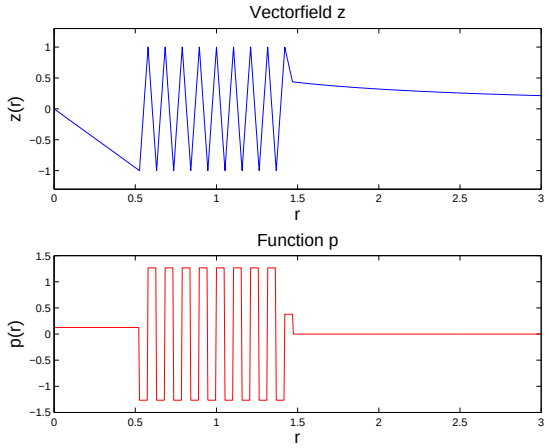

Figure 7: The function p and the vector field z (in fact $-z$ and p are displayed) constructed in the proof of Proposition 6.

3.2 ...and when it does not.

It should be observed that in the above example, in the original function f, there is some texture near the edge of the cartoon part (at $r = 1$). This is not a coincidence and the aim of this section is to prove that this property is necessary to obtain a perfect decomposition.

First, we consider the one-dimensional setting and we recall the argument given in [40]. Assume that we want to decompose a function $f \in L^1(\mathbb{R}) \cap L^2(\mathbb{R})$ using $(\mathcal{Q}_\lambda(f))$ (replacing $\mathrm{BV}(\mathbb{R}^2)$ with $\mathrm{BV}(\mathbb{R})$). The G-norm can be computed as

$$\|v\|_G = \inf_{C\in\mathbb{R}} \sup_{t\in\mathbb{R}} \left| \int_{-\infty}^{t} v(s)ds + C \right|.$$

The function $V : t \mapsto \int_{-\infty}^{t} v(s)ds$ is continuous, bounded (for $v \in L^1(\mathbb{R})$) and

the optimal C is $C = -\frac{\sup V + \inf V}{2}$. To fix ideas, let us consider a rectangular function perturbed with some textures (see Figure 8)

$$f(x) = \mathbf{1}_{(0,1)}(x) + \beta \sin(8p\pi x)\mathbf{1}_{\frac{1}{4}\leqslant|x|\leqslant\frac{3}{4}}.$$

The ideal decomposition one would expect is a perfect step $u(x) = \mathbf{1}_{(0,1)}(x)$,

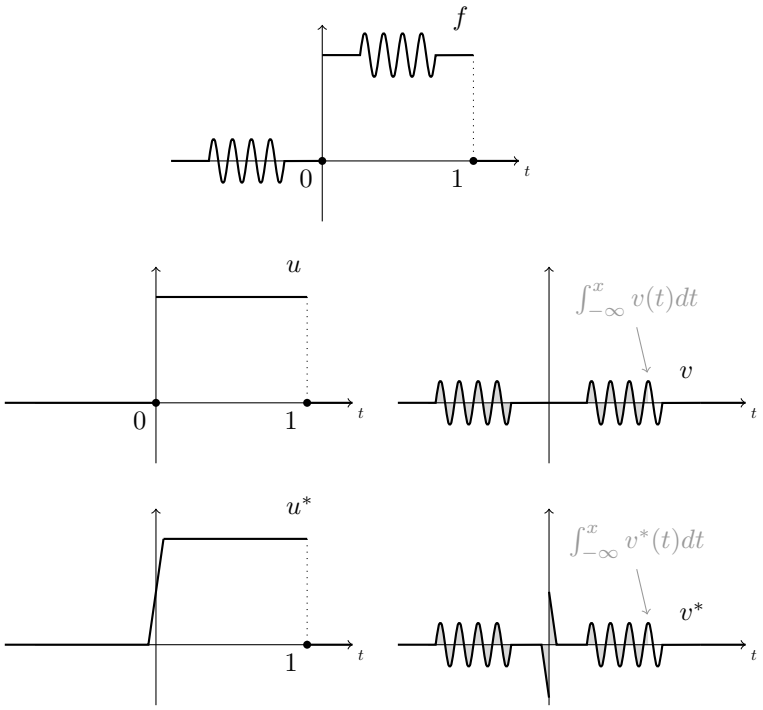

Figure 8: Top: original signal f. Middle row: expected decomposition. Bottom row: decomposition with the same energy.

and a pure oscillation $v(x) = \beta \sin(8p\pi x)\mathbf{1}_{\frac{1}{4}\leqslant|x|\leqslant\frac{3}{4}}$ (Figure 8, middle row).

The energy of the cartoon part is simply $\int |Du| = u(0^+) - u(0^-) + u(1^-) - u(1^+) = 2$, whereas the energy of the texture part is given by $\|v\|_G = \beta \int_{\frac{1}{4}}^{\frac{1}{4}+\frac{1}{8p}} \sin(8p\pi t)dt = \frac{\beta}{4p\pi}$. Yet, replacing u on $[-\frac{1}{4}, \frac{1}{4}]$ with any non-decreasing function u^* with the same limits at $\pm\frac{1}{4}$, say, a ramp $x \mapsto (\frac{1}{2} + \frac{1}{2\eta}x)\mathbf{1}_{[-\eta,\eta]}(x)$ as in Figure 8, last row), one still gets the same cartoon energy $\int |Du^*| = 2$. As for the texture part, we should notice that one extra oscillation is added near the discontinuity of the original function f. But since the G-norm favors oscillations, this change in the texture part is not penalized. Indeed,

$$\|v^*\|_G = \max\left(\frac{\beta}{4p\pi}, \int_{-\eta}^{0} (\frac{1}{2} + \frac{1}{2\eta}t)dt\right) = \frac{\beta}{4p\pi} \tag{26}$$

for η small enough ($0 \leqslant \eta \leqslant \min(\frac{1}{4}, \frac{\beta}{p\pi})$).

Therefore, we see on this example that *given any decomposition with sharp edges, there exists a decomposition with the same energy where halos around edges appear in the texture part.* This explains why some edges appear in the texture part in Figure 1. This phenomenon may also explain the kind of halo that appears in smooth areas: replacing the ramp with a slow gradation, one may alter smooth parts without changing the energy.

3.3 Texture near edges

In the above example we have observed that, *if the perfect decomposition were optimal*, another optimal decomposition would have "shadow edges" in the texture part: depending on luck or on the choice of the algorithm, this artifact may not appear.

Now we advocate the fact that in the two-dimensional framework, and for typical images of the model, *the artifact is bound to appear*: there should *always* be some texture in the v part around the points where u has jumps. One may prove (see [38] for the proof) that:

Proposition 7. *Let $f \in L^2(\mathbb{R}^2)$ be a radial function, $u = \mathbf{1}_{B(0,1)}$ and $v = f - \mathbf{1}_{B(0,1)}$ such that $v \neq 0$. Let $\varepsilon > 0$ and $C_{(-\varepsilon,\varepsilon)} = \{x \in \mathbb{R}^2,\ 1-\varepsilon < |x| < 1+\varepsilon\}$. If $v_{|\Omega_{(-\varepsilon,\varepsilon)}} = 0$, then the decomposition (u, v) is not optimal.*

More generally, for any convex set $C \subset \mathbb{R}^2$ and $\varepsilon > 0$, let us define

$$C_{-\varepsilon} = \{x \in C,\ d(x, \partial C) \geqslant \varepsilon\} \quad \text{and} \quad C_{-\varepsilon,\varepsilon} = \{x \in \mathbb{R}^2,\ d(x, \partial C) < \varepsilon\}.$$

The following result holds (see Proposition 5.2.14 in [38]):

Proposition 8. *Let $C \subset \mathbb{R}^2$ be a $C^{1,1}$ convex body, $f \in L^2(\mathbb{R}^2) \setminus \{\mathbf{1}_C\}$, $u = \mathbf{1}_C$ and $v = f - \mathbf{1}_C$. Assume that $\operatorname{Supp} v \subset \overline{C}$ and that the decomposition (u, v) is optimal. Then $\operatorname{Supp} v \cap \partial C \neq \emptyset$, where $\operatorname{Supp} v$ is the support of v.*

Proof. Assume by contradiction that $d(\operatorname{Supp} v, \partial C) > 0$, so that there exists $\varepsilon > 0$ such that $\operatorname{Supp} v \subseteq C_\varepsilon$. .

As (u, v) is optimal, equations (21), (22), (23) hold. Since $\frac{\int_{\mathbb{R}^2} pv}{\int |Dp|} = \|v\|_G = \sup_{w \in \mathrm{BV}(\mathbb{R}^2)\setminus 0} \frac{\int_{\mathbb{R}^2} wv}{\int |Dw|}$, p is a non-trivial minimizer of $G(w) := \int |Dw| - \int_{\mathbb{R}^2} \frac{v}{\|v\|_G} w$. The level sets $(E_t)_{t\in\mathbb{R}}$ of p are thus solutions to the prescribed mean curvature problem associated to $-\frac{v}{\|v\|_G}$:

$$\inf_{E \subset \mathbb{R}^2} \operatorname{Per} E - \int_E \frac{v}{\|v\|_G}.$$

Now, we replace p with $p^* = p\mathbf{1}_{C_\varepsilon}$, so that $\{p^* \geqslant t\} = E_t \cap C_\varepsilon$ for $t \geqslant 0$, and $\{p^* < t\} = E_t \cap C_\varepsilon$ for $t < 0$. Since C_ε is convex, $\operatorname{Per}(E_t \cap C_\varepsilon) \leqslant \operatorname{Per} E_t$, with strict inequality if $|E_t \setminus C_\varepsilon| > 0$.

By Lemma 1 below, $|Dp|(C_{(-\varepsilon,\varepsilon)}) > 0$, and the coarea formula implies that the set $B = \{t > 0,\ |E_t \cap C_{(-\varepsilon,\varepsilon)}| > 0\}$ has positive Lebesgue measure. Since

$\mathrm{Per}\,(E_t \cap C_\varepsilon) < \mathrm{Per}\,E_t$ for all $t \in B$, $\int |Dp^*| < \int |Dp|$. Since $\int p^* v = \int pv$, we see that $G(p^*) < G(p)$, which is a contradiction. □

The following lemma is a consequence of the Gauss-Green theorem (see [38, Lemma 5.2.13]):

Lemma 1. *Under the same assumptions as in Proposition 8, if p is the function defined in Equations* (22),(23) *and $\varepsilon > 0$, then $|Dp|(C_{(-\varepsilon,\varepsilon)}) > 0$.*

To conclude this section, let us observe that the TVL1 model is not concerned with such a limitation, as the following example shows (see [38] for the proof). Let $N \in \mathbb{N}^*$. For $2 \leqslant \lambda \leqslant 2N$, the radial function f defined by

$$\widetilde{f}(r) = \mathbf{1}_{[0,1]}(r) - \beta \sin(N\pi r)\mathbf{1}_{[2,3]}(r), \tag{27}$$

has an optimal decomposition given by:

$$\begin{aligned} \tilde{u}(r) &= \mathbf{1}_{[0,1]}(r), \\ \tilde{v}(r) &= -\beta \sin(N\pi r)\mathbf{1}_{[2,3]}(r). \end{aligned}$$

The corresponding decomposition is illustrated in Figure 9.

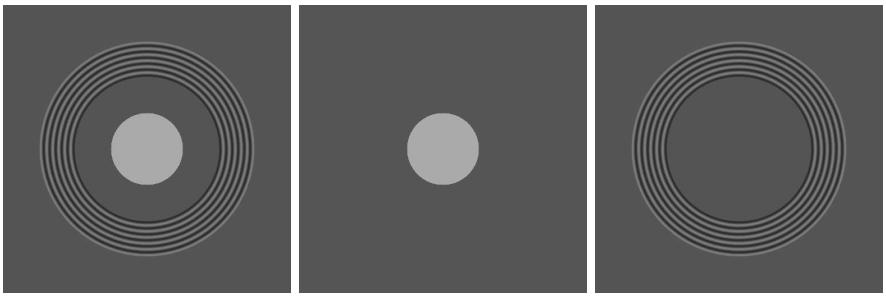

Figure 9: $TV - L^1$ decomposition predicted for (27): original image f (left), cartoon part $u = \mathbf{1}_{B(0,1)}$ (middle), texture part $v(x) = -\sin(N\pi|x|)\mathbf{1}_{[2,3]}(|x|)$ (right).

4 Conclusion

We have presented the analysis of the TVL1 and TV-G models developed in [38]. On the one hand, the behavior of the TVL1 model relies on geometric considerations. Our study shows the connection between the model and morphological openings. The decomposition produced by TVL1 is quite similar to granulometries, and the crucial notion to distinguish texture or noise from structure is the *scale*.

On the other hand, the key notion used by the TV-G model is the *oscillation* of a pattern. While in some cases the TV-G model is able to separate oscillating

textures from the geometric structure of images, we have highlighted a serious limitation of the model: in the original signal, there must be some texture in the neighborhood of edges for the decomposition to be perfect. Otherwise, shadows of edges or gradations appear in the texture part, resulting in an *inflated* aspect of the result.

Appendix

Proof of Proposition 6. We build the vector field z in (21) and the corresponding p in (23) using $\lambda\tilde{p} = \frac{1}{r}\frac{\partial}{\partial r}(r\tilde{z}(r))$.

For $r \in [0, r_{j^*}]$, we set $\tilde{z}(r) = (-1)^{j^*-1}\frac{r}{r_{j^*}}$, so that $\tilde{p}(r) = p_{j^*-1} = (-1)^{j^*-1}\frac{2}{\lambda r_{j^*}}$. By induction on k (with $j^* \leqslant k \leqslant k^* - 1$), we define $\tilde{z}$ on $[0, r_k]$ such that $\tilde{z}(r_k) = (-1)^{k-1}$. We set, for $r \in (r_k, r_{k+1}]$,

$$\begin{aligned}\tilde{z}(r) &= \frac{1}{r}\left(r_k\tilde{z}(r_k) + \frac{\lambda p_k}{2}(r^2 - r_k^2)\right) \quad \text{with } p_k := (-1)^k\frac{2}{\lambda(r_{k+1} - r_k)},\\ &= \frac{1}{r}\left((-1)^{k-1}r_k + (-1)^k\frac{r^2 - r_k^2}{r_{k+1} - r_k}\right),\end{aligned}$$

so that $\tilde{p}(r) = p_k$ and $\tilde{z}(r_{k+1}) = (-1)^k$.

For $r \in (r_{k^*}, +\infty)$, we set $\tilde{z}(r) = \frac{r_{k^*}\tilde{z}(r_{k^*})}{r} = (-1)^{k^*-1}\frac{r_{k^*}}{r}$, so that $\tilde{p}(r) = p_{k^*} := 0$.

Observe that the fact that $\tilde{z}(1) = \tilde{z}(r_0) = -1$ implies that $(z, Du) = |Du|$, $|Du|$-almost everywhere. Moreover, it is easy to check that the condition $r_{k+1} - r_k \leqslant r_k$ for $j^* \leqslant k \leqslant k^* - 1$ implies that $\tilde{z}$ varies monotonically from $(-1)^{k-1}$ to $(-1)^k$ in $[r_k, r_{k+1}]$. Hence we have built z and p which satisfy (21) and (23).

It remains to prove that p satisfies (22). The total variation of p is equal to

$$\begin{aligned}\int |Dp| &= 2\pi r_{j^*}|p_{j^*} - p_{j^*-1}| + \ldots + 2\pi r_k|p_k - p_{k-1}| + \ldots + 2\pi r_k^*|p_{k^*} - p_{k^*-1}|\\ &= 2\pi r_{j^*}\left(\frac{2}{\lambda r_{j^*}} + \frac{2}{\lambda(r_{j^*+1} - r_{j^*})}\right) + \ldots + 2\pi r_k\left(\frac{2}{\lambda(r_k - r_{k-1})} + \frac{2}{\lambda(r_{k+1} - r_k)}\right)\\ &\quad + \ldots + 2\pi r_k^*\left(\frac{2}{\lambda(r_{k^*} - r_{k-1})} + 0\right)\\ &= \frac{4\pi}{\lambda}\left(1 + \sum_{k=j^*}^{k^*-1}\frac{r_{k+1} + r_k}{r_{k+1} - r_k}\right).\end{aligned}$$

Hence, choosing $\lambda = 4\pi\left(1 + \sum_{k=j^*}^{k^*-1}\frac{r_{k+1}+r_k}{r_{k+1}-r_k}\right)$, we obtain that $\int |Dp| = 1$. Moreover the vector field g is such that $\|g\|_\infty = \|v\|_G$. Indeed, by symmetry, there exists an optimal vector field g^* which is radial, and the difference $g - g^*$ is radial and divergence free, hence of the form $\frac{C}{r}$. Since both g and g^* are bounded, we get $C = 0$ and $g = g^*$. Observing that $\tilde{g}(r_k) = (-1)^{k+1}\|g\|_\infty = -\frac{Dp}{|Dp|}(\{r_k\})\|g\|_\infty$, we obtain (24) and thus (22).

As a conclusion, we obtain that the decomposition (u, v) is optimal for $(\mathcal{Q}_\lambda(f))$ with $\lambda = 4\pi\left(1 + \sum_{k=j^*}^{k^*-1} \frac{r_{k+1}+r_k}{r_{k+1}-r_k}\right)$. It is not difficult to see that it is also optimal for $\lambda = 4\pi$ (consider $\tilde{z}(r) = r$ for $0 \leqslant r \leqslant 1$, $\frac{1}{r}$ otherwise, and $\tilde{p} = \frac{2}{\lambda}\mathbf{1}_{(0,1)}$). Consequently, it is optimal for all λ such that $4\pi \leqslant \lambda \leqslant 4\pi\left(1 + \sum_{k=j^*}^{k^*-1} \frac{r_{k+1}+r_k}{r_{k+1}-r_k}\right)$.

□

References

[1] Allard, W. (2007). Total variation regularization for image denoising I: Geometric theory. *SIAM Journal on Mathematical Analysis*, 39(4):1150–1190.

[2] Allard, W. (2008). Total variation regularization for image denoising II: Examples. *SIAM Journal on Imaging Sciences*, 1(4):400–417.

[3] Allard, W. (2009). Total variation regularization for image denoising III: Examples. *SIAM Journal on Imaging Sciences*, 2(2):532–568.

[4] Alliney, S. (1992). Digital filters as absolute norm regularizers. *IEEE Transactions on Signal Processing*, 40(6):1548–1562.

[5] Alliney, S. (1996). Recursive median filters of increasing order : a variational approach. *IEEE Transactions on Signal Processing*, 44(6):1346–1354.

[6] Alter, F. and Caselles, V. (2009). Uniqueness of the cheeger set of a convex body. *Nonlinear Analysis: Theory, Methods & Applications*, 70(1):32–44.

[7] Alter, F., Caselles, V., and Chambolle, A. (2005a). A characterization of convex calibrable sets in $\mathbb{R}^N$. *Math. Ann.*, 7:29–53.

[8] Alter, F., Caselles, V., and Chambolle, A. (2005b). Evolution of convex sets in the plane by minimizing the total variation flow. *Interfaces and Free Boundaries*, 332:329–366.

[9] Alvarez, L., Guichard, F., Lions, P.-L., and Morel, J.-M. (1993). Axioms and fundamental equations of image processing. *Archive for Rational Mechanics and Analysis*, 123:199–257. 10.1007/BF00375127.

[10] Ambrosio, L. (1997). *Corso introduttivo alla teoria geometrica della misura ed alle superfici minimime*. Quad. Scuola Norm. Sup. Pisa. Pantograph, Genova.

[11] Ambrosio, L., Fusco, N., and Pallara, D. (2000). *Functions of Bounded Variation and Free Discontinuity Problems*. Oxford mathematical monographs. Oxford University Press.

[12] Andreu, F., Ballester, C., Caselles, V., and Mazón, J. M. (2001a). The dirichlet problem for the total variation flow. *Journal of Functional Analysis*, 180(2):347–403.

[13] Andreu, F., Ballester, C., Caselles, V., and Mazón, J. M. (2001b). Minimizing total variation flow. *Differential and Integral Equations*, 14(3):321–360.

[14] Andreu, F., Caselles, V., Diaz, J. I., and Mazón, J. M. (2002). Some qualitative properties for the total variation flow. *Journal of Functional Analysis*, 188(2):516 – 547.

[15] Andreu-Vaillo, F., Caselles, V., and Mazón, J. M. (2002). *Parabolic quasilinear equations minimizing linear growth functionals*, volume 223 of *Progress in Mathematics*. Birkhauser.

[16] Anzellotti, G. (1983). Pairing between measures and bounded functions and compensated compactness. *Ann. di Matematica Pura ed Appl.*, IV(135):293–318.

[17] Aubert, G. and Aujol, J. (2005). Modeling very oscillating signals. Application to image processing. *Applied Mathematics and Optimization*, 51(2).

[18] Aujol, J.-F., Aubert, G., Blanc-Féraud, L., and Chambolle, A. (2005). Image decomposition into a bounded variation component and an oscillating component. *Journal of Mathematical Imaging and Vision*, 22(1):71–88.

[19] Aujol, J.-F. and Chambolle, A. (2005). Dual norms and image decomposition models. *International Journal of Computer Vision*, 63(1):85–104.

[20] Aujol, J.-F. and Gilboa, G. (2006). Constrained and SNR-based solutions for TV-Hilbert space image denoising. *Journal of Mathematical Imaging and Vision*, 26(1-2):217–237.

[21] Ballester, C., Caselles, V., and Monasse, P. (2003). The tree of shapes of an image. *ESAIM: Control, Optimisation and Calculus of Variations*, 9:1–18.

[22] Bellettini, G., Caselles, V., and Novaga, M. (2002). The total variation flow in $\mathbb{R}^N$. *J. Differential Equations*, 184(2):475–525.

[23] Bellettini, G., Caselles, V., and Novaga, M. (2005). Explicit solutions of the eigenvalue problem $div\left(\frac{Du}{|Du|}\right) = u$ in $\mathbb{R}^2$. *SIAM J. Math. Anal.*, 36:1095–1129.

[24] Bellettini, G., Novaga, M., and Paolini, M. (2001). Characterization of facet–breaking for nonsmooth mean curvature flow in the convex case. *Interfaces and Free Boundaries*, 3:415–446.

[25] Beucher, S. and Lantuéjoul, C. (1979). Use of watersheds in contour detection. In *International workshop on image processing, real-time edge and motion detection*.

[26] Bouraoui, B., Ronse, C., Baruthio, J., Passat, N., and Germain, P. (2008). Fully automatic 3d segmentation of coronary arteries based on mathematical morphology. In *ISBI 2008, 5th International Symposium on Biomedical Imaging: From Nano to Macro*, pages 1059–1062. IEEE.

[27] Carlier, G., Comte, M., and Peyré, G. (2009). Approximation of maximal cheeger sets by projection. *ESAIM: Mathematical Modelling and Numerical Analysis*, 43(1):131–150.

[28] Caselles, V., Chambolle, A., and Novaga, M. (2007). The discontinuity set of solutions of the tv denoising problem and some extensions. *Multiscale Modeling and Simulation*, 6(3):879–894.

[29] Caselles, V., Chambolle, A., and Novaga, M. (2008). Some remarks on uniqueness and regularity of cheeger sets.

[30] Caselles, V. and Monasse, P. (2009). *Geometric Description of Images As Topographic Maps*. Springer Publishing Company, Incorporated, 1st edition.

[31] Caselles, V., Novaga, M., and Pöschl, C. (2012). Tv denoising of the characteristic function of two balls in the plane. submitted to Inverse Problems and Imaging.

[32] Chambolle, A. (2004). An algorithm for mean curvature motion. *Interfaces Free Bound.*, 6(2):195–218.

[33] Chambolle, A., Caselles, V., Novaga, M., Cremers, D., and Pock, T. (2009). An introduction to Total Variation for Image Analysis.

[34] Chan, T. and Esedoglu, S. (2005). Aspects of total variation regularized L^1 function approximation. *SIAM Journal on Applied Mathematics*, 65(5):1817–1837.

[35] Cheng, F. and Venetsanopoulos, A. N. (1992). An adaptive morphological filter for image processing. *IEEE Trans. Image Process.*, 1:533–539.

[36] Darbon, J. (2005). Total variation minimization with L^1 data fidelity as a contrast invariant filter. *4th International Symposium on Image and Signal Processing and Analysis (ISPA 2005)*, pages 221–226.

[37] Darbon, J. and Sigelle, M. (2006). Image restoration with discrete constrained total variation part I: Fast and exact optimization. *Journal of Mathematical Imaging and Vision*, 26(3):261–276.

[38] Duval, V. (2011). *Variational and non-local methods in image processing: a geometric study*. PhD thesis, Telecom ParisTech, `https://www.ceremade.dauphine.fr/~vduval/files/these_fr.pdf`.

[39] Duval, V., Aujol, J.-F., and Gousseau, Y. (2009). The TVL1 Model: a Geometric Point of View. *Multiscale Model. Simul.*, 8(1):154–189.

[40] Duval, V., Aujol, J.-F., and Vese, L.-A. (2010). Mathematical modeling of textures: Application to color image decomposition with a projected gradient algorithm. *Journal of Mathematical Imaging and Vision*, 37:232–248.

[41] Garnett, J., Le, T., Meyer, Y., and Vese, L. (2007). Image decompositions using bounded variation and generalized homogeneous besov spaces. *Appl. Comput. Harmon. Anal.*, 23:25–56.

[42] Gilles, J. (2007). Noisy image decomposition: a new structure, texture and noise model based on local adaptivity. *Journal of Math. Imag. and Vision (JMIV)*, 28(3):285–295.

[43] Gilles, J. (2009). Image decomposition: Theory, numerical schemes, and performance evaluation. *Advances in Imaging and Electron Physics*, 158:89–137.

[44] Guichard, F., Morel, J.-M., and Ryan, R. (2004). Contrast invariant image analysis and PDE's. preprint.

[45] Haas, A., Matheron, G., and Serra, J. (1967). Morphologie mathématique et granulométries en place. *Annales des Mines*, 11:736–753.

[46] Haddad, A. (2007). Texture separation: $BV - G$ and $BV - L^1$ models. *Multiscale Modeling and Simulation*, 6(1):273–286.

[47] Haddad, A. and Meyer, Y. (2007). An improvement of rudin-osher-fatemi model. *Applied and Computational Harmonic Analysis*, 22(3):319 – 334.

[48] Hanbury, A. and Serra, J. (2002). Analysis of oriented textures using mathematical morphology. In *in OAGM*, pages 49–52.

[49] Kawohl, B. and Lachand-Robert, T. (2006). Characterization of cheeger sets for convex subsets of the plane. *Pacific J. Math.*, 225(1):103–118.

[50] Kim, Y. and Vese, L. (2009). Image recovery using functions of bounded variation and sobolev spaces of negative differentiability. *Inverse Problems and Imaging*, 3:43–68.

[51] Kindermann, S., Osher, S., and Xu, J. (2006). Denoising by bv-duality. *J. Sci. Comput.*, 28:411–444.

[52] Le, T. and Vese, L. (2005). Image decomposition using total variation and div(bmo). *Multiscale Modeling and Simulation*, 4(2):390–423.

[53] Lieu, L. and Vese, L. (2009). Image restoration and decomposition via bounded total variation and negative Hilbert-Sobolev spaces. *Applied Mathematics & Optimization*, 58:167–193.

[54] Matheron, G. (1964). Etude théorique des granulométries. Technical Report 57, Ecole des Mines de Paris.

[55] Matheron, G. (1975). *Random Sets and Integral Geometry*. John Wiley & Sons, New York.

[56] Matheron, G. and Serra, J. (2002). The birth of mathematical morphology. In Talbot, H. and Beare, R., editors, *Mathematical Morphology and its application to Image and Signal Processing (ISMM 2002)*, pages 1–16, Sidney.

[57] Meyer, Y. (2001). *Oscillating patterns in image processing and nonlinear evolution equations*, volume 22 of *University Lecture Series*. American Mathematical Society, Providence, RI. The fifteenth Dean Jacqueline B. Lewis memorial lectures.

[58] Monasse, P. and Guichard, F. (2000). Scale-space from a level lines tree. *Journal of Visual Communication and Image Representation*, 11(2):224 – 236.

[59] Morgan, S. and Vixie, K. (2007). L^1TV computes the flat norm for boundaries. *Abstract and Applied Analysis*, 2007. Article ID 45153, doi:10.1155/2007/45153.

[60] Nikolova, M. (2002). Minimizers of cost-functions involving non-smooth data-fidelity terms. application to the processing of outliers. *SIAM Journal on Numerical Analysis*, 40(3):965–994.

[61] Nikolova, M. (2004a). A variational approach to remove outliers and impulse noise. *JMIV*, 20(1-2):99–120.

[62] Nikolova, M. (2004b). Weakly constrained minimization. application to the estimation of images and signals involving constant regions. *Journal of Mathematical Imaging and Vision*, 21(2):155–175.

[63] Osher, S., Sole, A., and Vese, L. (2003). Image decomposition and restoration using total variation minimization and the H^{-1} norm. *SIAM journal on Multiscale Modeling and Simulation*, 1(3):349–370.

[64] Rudin, L., Osher, S., and Fatemi, E. (1992). Nonlinear total variation based noise removal algorithms. *Physica D*, 60:259–268.

[65] Serra, J. (1982). *Image Analysis and Mathematical Morphology*. Academic Press, San Diego, CA.

[66] Serra, J. (1988). *Image Analysis and Mathematical Morphology. Volume 2: Theoretical Advances*. Academic Press.

[67] Soille, P. (2003). *Morphological Image Analysis: Principles and Applications*. Springer-Verlag New York, Inc., Secaucus, NJ, USA.

[68] Vanrell, M. and Vitria, J. (1993). Mathematical morphology, texture perception and granulometries. In *SPIE Image Algebra and Morphological Image Proceessing IV*, pages 152–161.

[69] Vese, L. and Osher, S. (2003). Modeling textures with total variation minimization and oscillating patterns in image processing. *Journal of Scientific Computing*, 19:553–572.

[70] Vincent, L. (1993). Grayscale area openings and closings, their efficient implementation and applications. In Serra, J. and Salembier, P., editors, *Proceedings of the 1st Workshop on Mathematical Morphology and its Applications to Signal Processing*, pages 22–27, Barcelona, Spain.

[71] Vixie, K., Clawson, K., Asaki, T., Sandine, G., Morgan, S., and Price, B. (2010). Multiscale flat norm signature for shapes and images. *Applied Mathematical Sciences*, 4(14):667–680.

[72] Vixie, K. and Esedoglu, S. (2007). Some properties of minimizers for the Chan-Esedoglu L^1TV functional. Technical report, arXiv [http://arXiv.org/oai2] (United States).

[73] Yin, W., Goldfarb, D., and Osher, S. (2007a). A comparison of three total variation based texture extraction models. *Journal of Visual Communication and Image Representation*, 18(3):240–252.

[74] Yin, W., Goldfarb, W., and Osher, S. (2007b). The total variation regularized L^1 model for multiscale decomposition. *SIAM Journal on Multiscale Modeling and Simulation*, 6(1):190–211.